6

Collective instability

The term collective instability refers to a spontaneous excitation of gravity waves by a fully developed and initially homogeneous field of salt fingers. This effect, briefly mentioned in Chapter 3, was discovered by Stern (1969). Stern's theory was inspired by laboratory experiments with salt fingers in uniform background property gradients. In these experiments (some of which are described in Stern and Turner, 1969) large-scale waves appeared shortly after the development of salt fingers and were followed by even more dramatic transformation of the flow into a series of alternating convective cells and sharp interfaces – structures that came to be known as thermohaline staircases (Chapter 8). Ironically, the link between waves and staircases, which motivated the collective instability theory in the first place, has never been confirmed. These effects are largely independent. Nevertheless, collective instability turned out to be a very interesting phenomenon in its own right, profoundly affecting doubly diffusive fluids in a number of ways.

At least three different theoretical models (Stern, 1969; Holyer, 1981; Stern *et al.*, 2001) have been proposed to explain the generation of large-scale waves by fingers. While each model is based on distinct physics, they all lead to the same conclusion – collective instability is controlled by the Stern number:

$$A = \frac{\alpha F_T - \beta F_S}{\nu(\alpha \bar{T}_z - \beta \bar{S}_z)}. \tag{6.1}$$

An equivalent expression for A in terms of the density flux is given in (3.5). All three models are summarized and compared next (Section 6.1), followed by a more in-depth discussion of the parametric theory (Stern *et al.*, 2001) in Section 6.2.

6.1 Approaches

The first argument was proposed by Stern (1969). Stern assumed that the coupling between large-scale waves and fingers in the laboratory experiments (Stern and

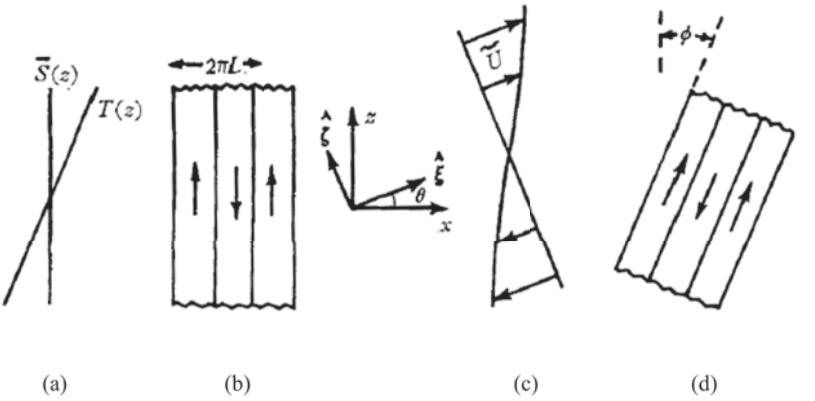

Figure 6.1 Stern's (1969) model. Stern envisioned initially vertical salt fingers in the uniform temperature and salinity gradient (a,b), which are subjected to the shear of a large-scale gravity wave (c). The wave slightly tilts the fingers (d) reducing their vertical transport of heat, salt and, ultimately, buoyancy. The buoyancy perturbation, in turn, affects the gravity wave. The feedback between the fingers and wave results in the amplification of the latter, provided that the Stern number (6.1) exceeds unity. From Stern (1969).

Turner, 1969) is due to the ability of the wave shear to tilt fingers, thereby reducing the vertical component of heat and salt fluxes, as indicated in Figure 6.1. The associated large-scale modulation of the vertical transport results in temperature and salinity convergences which, in turn, modify the buoyancy distribution in the wave. Stern argued that the buoyancy forcing induced in this manner provides a feedback mechanism for the amplification of gravity waves as long as A exceeds unity.

Stern's model was reexamined by Holyer (1981). Of particular concern was the ad hoc assumption that tilting of fingers reduces the vertical components of the temperature and salinity fluxes but not their magnitudes. Holyer (1981) offered a more mathematically rigorous, if not more physical, treatment of the collective instability using multiscale analysis. She examined stability of the two-dimensional basic state consisting of an array of steady, vertical fingers with respect to long-wavelength perturbations, as illustrated in Figure 6.2. The resulting condition for instability was $A > 1/3$, which is similar, but not identical, to Stern's (1969) criterion ($A > 1$). Holyer (1985) reproduced this calculation in three dimensions, assuming a square horizontal planform of salt fingers, and arrived at the collective instability criterion of $A > 2/3$ – even closer to Stern's original prediction. While Holyer's models avoided questionable steps in the original theory, they were replaced by other assumptions that were also not fully justified. In particular, salt

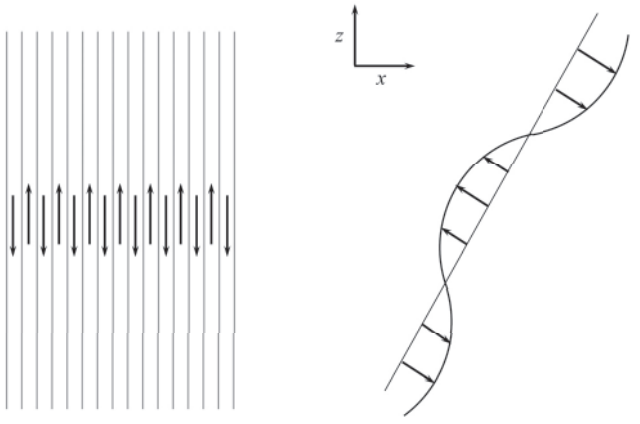

(a) (b)

Figure 6.2 Schematic illustration of Holyer's (1984) model. Holyer analyzed stability of the marginally unstable vertical fingers (a) with respect to large-scale perturbations (b). From Holyer (1984).

fingers observed in nature or in laboratory settings are not vertical and definitely not steady. As discussed in Chapter 2, the dominant horizontal wavelength realized in a fully developed salt-finger field corresponds much better to the linearly fastest growing mode than to the steady solution used by Holyer (1981, 1985).

A third attempt to formulate a rigorous theory for the collective instability was made by Stern *et al.* (2001). The vertical temperature and salinity fluxes due to salt fingers were assumed to be controlled by the large-scale T–S gradients and parameterized accordingly:

$$\begin{cases} F_T = -K_T(R_\rho)\frac{\partial T}{\partial z}, \\ F_S = -K_S(R_\rho)\frac{\partial S}{\partial z}. \end{cases} \tag{6.2}$$

The flux ratio $\gamma = \frac{\alpha F_T}{\beta F_S}$ was approximated by a constant and the effects of shear on the fluxes – the essential element of the Stern (1969) model – were ignored based on compelling numerical evidence. The amplification of the gravity wave was attributed to subtle changes in the large-scale buoyancy distribution, resulting from the convergence of the vertical double-diffusive fluxes (6.2). Remarkably, linear stability analysis of the parameterized flux-gradient system recovered Stern's original instability condition: $A > 1$. Theoretical predictions of the wave growth rates were confirmed quantitatively by DNS. The very reasonable physical assumptions, its performance and utility warrant a closer look at the flux-gradient model (Stern *et al.*, 2001), which is next discussed in greater detail.

6.2 Parametric flux-gradient model

The collective instability model in Stern *et al.* (2001) is based on the Navier–Stokes equations for the large-scale (relative to individual fingers) flow components. The model assumes a horizontally homogeneous background state, which makes it possible to focus on two-dimensional (x,z) solutions without any loss of generality. In order to reduce the number of governing parameters, we use the standard double-diffusive non-dimensionalization (1.11) introduced in Chapter 1. The non-dimensional expression for double-diffusive fluxes in (6.2) becomes

$$\begin{cases} F_T = -Nu(R_\rho)\dfrac{\partial T}{\partial z}, \\ F_S = \dfrac{F_T}{\gamma(R_\rho)}, \end{cases} \tag{6.3}$$

where, as previously (Chapter 3) we assumed that the Nusselt number (Nu) and the flux ratio (γ) are controlled by the density ratio (R_ρ). The governing equations are linearized with respect to uniform vertical temperature–salinity gradients:

$$\begin{cases} \dfrac{\partial}{\partial t}T' + \dfrac{\partial \psi'}{\partial x} = -\dfrac{\partial}{\partial z}F'_T, \\ \dfrac{\partial}{\partial t}S' + \dfrac{1}{R_\rho}\dfrac{\partial \psi'}{\partial x} = -\dfrac{\partial}{\partial z}F'_S, \\ \dfrac{1}{Pr}\dfrac{\partial}{\partial t}\nabla^2\psi' = \left(\dfrac{\partial T'}{\partial x} - \dfrac{\partial S'}{\partial x}\right) + \nabla^4\psi', \end{cases} \tag{6.4}$$

where (F'_T, F'_S) in (6.4) are the linear perturbations of the temperature and salinity fluxes, and ψ' is the perturbation streamfunction, defined by $(u', w') = (-\psi'_z, \psi'_x)$. The non-dimensional expression for the temperature flux reduces to $F_T = -Nu(R_\rho)(1 + T'_z)$ and therefore

$$F'_T = -\left(\left.\frac{\partial Nu}{\partial R_\rho}\right|_{R_\rho=\bar{R}_\rho} R'_\rho + Nu(\bar{R}_\rho)T'_z\right), \tag{6.5}$$

where $\bar{R}_\rho$ is the basic density ratio and R'_ρ is the perturbation:

$$R'_\rho = \frac{(1 + T'_z)}{(\bar{R}_\rho^{-1} + S'_z)} - \bar{R}_\rho \approx \bar{R}_\rho\left(T'_z - \bar{R}_\rho S'_z\right). \tag{6.6}$$

The explicit expression for F'_S is obtained by expressing the salt flux in terms of the flux ratio as in (6.3), which after linearization yields

$$F'_S = \frac{F'_T}{\gamma(\bar{R}_\rho)} + \left.\frac{\partial \gamma^{-1}}{\partial R_\rho}\right|_{R_\rho=\bar{R}_\rho} R'_\rho Nu(\bar{R}_\rho). \tag{6.7}$$

Stability properties of the resulting linear system are analyzed using normal modes:

$$\begin{pmatrix} T' \\ S' \\ \psi' \end{pmatrix} = \begin{pmatrix} \hat{T} \\ \hat{S} \\ \hat{\psi} \end{pmatrix} \exp(ikx + imz + \lambda t), \tag{6.8}$$

substitution of which into (6.4)–(6.7) yields a cubic equation for the growth rate:

$$\lambda^3 + a_2\lambda^2 + a_1\lambda + a_0 = 0. \tag{6.9}$$

The coefficients of (6.9) are represented by lengthy algebraic expressions in terms of

$$a_i = a_i\left[k, m, \bar{R}_\rho, Nu(\bar{R}_\rho), \gamma(\bar{R}_\rho), A_{Nu}, A_\gamma\right], \tag{6.10}$$

where $A_{Nu} = \bar{R}_\rho \left.\frac{\partial Nu}{\partial R_\rho}\right|_{R_\rho=\bar{R}_\rho}$ and $A_\gamma = \bar{R}_\rho \left.\frac{\partial \gamma^{-1}}{\partial R_\rho}\right|_{R_\rho=\bar{R}_\rho}$ measure the variation in fluxes with the density ratio. It is interesting to note that the variation in the flux ratio (A_γ term) has a very limited effect on the collective instability. In the original paper (Stern *et al.*, 2001), the flux ratio was assumed to be constant ($A_\gamma = 0$). In retrospect, it is clear that setting A_γ to zero was just a lucky shot that, fortunately, did not introduce any significant errors in the analysis of the collective instability. For other forms of secondary double-diffusive instabilities (Chapters 7 and 8) the variation in the flux ratio becomes essential.

To formulate an explicit condition for the collective instability on the basis of (6.9) we note that the marginal stability point corresponds to a purely imaginary growth rate

$$\lambda = i\omega, \tag{6.11}$$

where ω is real. Next, (6.11) is substituted in the growth rate equation (6.9). Taking the real and imaginary components of the result, we obtain $\omega^2 = a_1$ and $a_2\omega^2 = a_0$, respectively, or

$$a_2 a_1 = a_0. \tag{6.12}$$

Using a sequence of algebraic inequalities, Stern *et al.* (2001) demonstrated that the critical condition for instability (6.12) can only be achieved if

$$\frac{Nu(\bar{R}_\rho)}{Pr}\frac{\gamma^{-1} - 1}{1 - \bar{R}_\rho^{-1}} > 1. \tag{6.13}$$

Expressing (6.13) in terms of the dimensional temperature and salinity fluxes and gradients, we recover Stern's original criterion for instability:

$$A = \frac{\alpha F_{T\,\mathrm{dim}} - \beta F_{S\,\mathrm{dim}}}{\nu(\alpha \bar{T}_{z\,\mathrm{dim}} - \beta \bar{S}_{z\,\mathrm{dim}})} > 1. \tag{6.14}$$

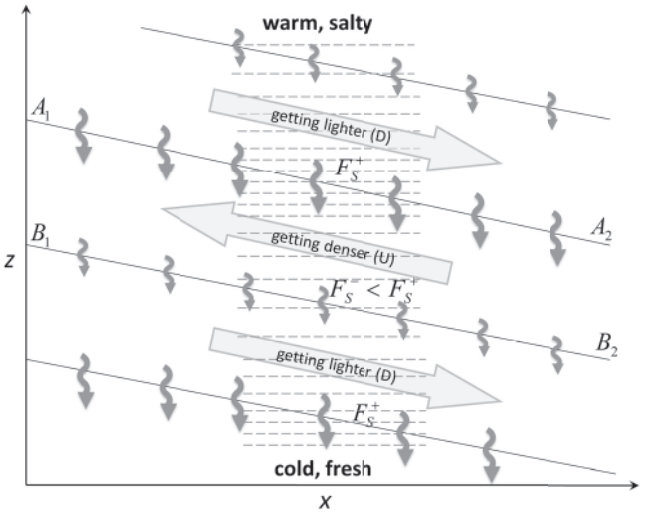

Figure 6.3 Physical mechanism of the collective instability in the Stern *et al.* (2001) parametric model. The instability is driven by the interplay between changes in stratification caused by the wave and the resulting spatial variation in the salt-finger buoyancy flux. After Stern *et al.* (2001).

6.3 Physical interpretation

The mechanism of the collective instability is physically explained in the schematic in Figure 6.3, which shows a plane internal gravity wave inclined at a small angle to the horizontal. In the upward-moving regions (U in Fig. 6.3) cold and fresh waters are advected from below across the mean isohalines and isotherms, locally decreasing temperature and salinity. Regions that are moving downward (D in Fig. 6.3) increase temperature and salinity by transporting relatively warm and salty water from above. Such a perturbation increases the vertical temperature and salinity gradients (T_z, S_z) in areas located below downward-flowing currents (D) and above the upward-moving ones (U), such as the front (A_1, A_2) in Figure 6.3. In regions immediately above the downward currents (D) – front (B_1, B_2) for instance – the gradients are reduced. The local increase (decrease) of temperature and salinity gradients results in larger (smaller) temperature and salinity fluxes. Since the salinity component of the salt-finger density flux exceeds its temperature component ($\gamma < 1$), the density flux is controlled by salinity. As a result, the density flux is distributed (Fig. 6.3) in a manner that tends to increase density in downward-flowing regions (D) and decrease it in the U-regions. Thus, the buoyancy forcing due to salt fingers has an adverse effect on the flow: forcing is downward when the velocity is upward and vice versa. Such systems are often susceptible to oscillatory "overstable" instabilities. Whether or not this mechanism leads to

instability depends on the balance between the buoyancy forcing by salt fingers and viscous damping, which is quantified by the Stern number (A). If $A > 1$, viscous dissipation plays a secondary role and the wave amplifies.

It is instructive to point out a formal analogy between the mechanisms of collective instability and laminar diffusive instability (Chapter 2). The eddy diffusivity of salt due to salt fingers exceeds the eddy diffusivity of temperature, as can be ascertained by taking the ratio of the two equations in (6.2):

$$\frac{K_T}{K_S} = \frac{\gamma}{R_\rho} < 1. \tag{6.15}$$

Thus, in fully developed salt fingering, the faster diffuser is salinity and the slower diffuser is temperature. The configuration in which the stably stratified component diffuses more slowly than the unstable one leads to the oscillatory diffusive instability. This is exemplified by the laminar case of cold and fresh water above warm and salty. Thus, by appealing to the analogy between turbulent and laminar fluids, we immediately arrive at the possibility of large-scale oscillatory instability in the salt-finger case. Note that temperature and salinity switch their roles as faster and slower diffusers depending on whether we consider molecular effects at the microscale or turbulent large-scale processes. The parallel between laminar diffusive convection and turbulent salt fingering could be made more quantitative by noting that the condition for oscillatory instability in diffusive systems is determined by the Prandtl number (Chapter 2). The smaller Pr, the more unstable is the system. For the turbulent salt-finger case, the relevant Prandtl number is based on turbulent diffusivity: $Pr_{\text{turb}} = \frac{\nu}{K_T} = \frac{\nu \bar{T}_Z}{F_T} \sim \frac{\nu \bar{\rho}_z}{F_\rho} = \frac{1}{A}$, which leads to the same conclusion as was rigorously derived in (6.14) – collective instability is controlled by the Stern number A.

Having examined the parametric flux-gradient theory, one might want to have a second look at the earlier attempts (Stern, 1969; Holyer, 1981, 1985) to formulate physical models of the collective instability. Focused on seemingly different driving processes, each model still managed to predict correctly the instability condition. Is there a deep reason for their success or was it largely coincidental? This question is more complicated than it appears at first. The non-dimensional parameter A is clearly an important one – it reflects the balance between the advective transfer and viscous damping; it can be thought of as the double-diffusive equivalent of the Reynolds number. Thus, it is possible that A should inevitably emerge as a critical collective instability condition in any sensible physical model, regardless of the specific assumptions. On the other hand, an in-depth analysis of the problem may reveal hidden analogies between the finger tilt (Stern, 1969), long-wave instabilities of the elevator modes (Holyer, 1981, 1985) and flux-gradient effects (Stern *et al.*, 2001), unifying different approaches to the collective instability. Borrowing one of

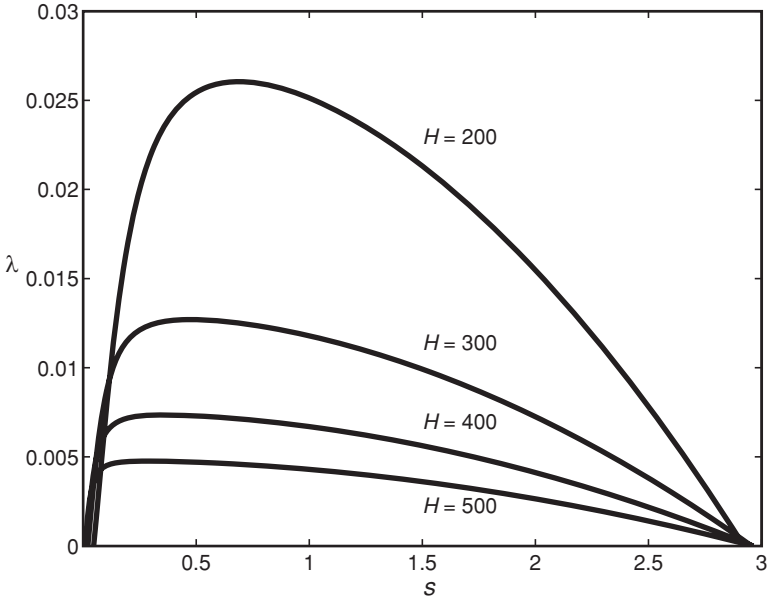

Figure 6.4 Growth rates of the collective instability waves as a function of the (non-dimensional) vertical wavelength (H) and the slope of the wave (s).

Stern's expressions, as memorable and original as his science, we can claim that each approach "has a certain degree of independent plausibility."

6.4 Specific solutions

The flux-gradient model (Stern *et al.*, 2001) not only explains the dynamics of collective instability but also affords quantitative and testable predictions for such major instability characteristics as the growth rates and dominant spatial patterns. These specific solutions, however, require knowledge of the salt-finger diffusivities of heat and salt and, in particular, of their dependence on the background density ratio. Due to computational constraints, Stern *et al.* (2001) based their analysis on diffusivities derived from two-dimensional numerical solutions. Since three-dimensional simulations for the heat–salt parameters ($\tau = 0.01$, $Pr = 7$) have recently become possible (e.g., Radko and Smith, 2012), we now reproduce several calculations in Stern *et al.* (2001) using the updated flux-gradient laws.

Simulations in Radko and Smith (2012) led to the parameterization (3.10) of the vertical temperature and salinity fluxes, which was used in (6.9) and (6.10) to evaluate the growth rate of the collective instability (λ). In Figure 6.4, λ is plotted as a function of the wave slope $\left(s = -\frac{k}{m}\right)$ for various values of the vertical wavelength

(H) and $R_\rho = 2$. Note that the system is invariant with respect to changes in the sign of the wave slope – the growth rates of the modes sloping downward in the positive x-direction (as in Fig. 6.3) are identical to those of the corresponding modes sloping upward, and therefore only positive slopes are shown in Figure 6.4. This convenient property does not apply to systems characterized by the presence of horizontal gradients of temperature and salinity (discussed in Chapter 7).

The results in Figure 6.4 indicate that the growth rates generally decrease with increasing H. The patterns of $\lambda(s)$ are similar for various values of H; they are characterized by a well-defined maximum at small but finite values of slope ($s = s_{\max}$). As H increases, this preferred maximal value of slope shifts towards lower values. The reader is reminded that the non-dimensionalization in Figure 6.4 is based on the salt-finger scale $d = \left(\frac{k_T \nu}{g\alpha|T_z|}\right)^{\frac{1}{4}} \sim 0.01$ m and $k_T \approx 1.4 \cdot 10^{-7}$ m^2 s^{-1}. Thus, vertical wavelengths of $H = 200$–500 in Figure 6.4 correspond to the dimensional range of 2–5 m. The non-dimensional growth rates of $\lambda = 0.005$–0.025 translate to $\lambda_{\text{dim}} = \frac{k_T}{d^2}\lambda = (7 - 35) \cdot 10^{-6}$ s^{-1} with the corresponding growth period of several hours.

In Figure 6.5 we plot the (real part of) growth rates as a function of k and m in logarithmic coordinates for various density ratios. While the range of unstable wavenumbers is only weakly dependent on the density ratio, the growth rates rapidly decrease with increasing R_ρ. For $R_\rho > 4.362$, the system becomes stable with respect to the collective instability. Note also that the application of the parametric instability implies scale separation between the wave and individual fingers. Thus, the accuracy of the model becomes questionable for relatively large k and m.

6.5 Nonlinear effects

The predictions of the parametric flux-gradient theory were validated by DNS in Stern *et al.* (2001). These simulations demonstrated that salt-finger fluxes are not strongly affected by large-scale wave shear despite the significant tilt of fingers, apparent in Figure 6.6. The momentum transfer by salt fingers, not taken into account by the parametric theory, was also confirmed to be of secondary importance and the finite amplitude perturbations amplify at rates consistent with the prediction in (6.9) and (6.10). Collective instabilities generally equilibrate only after development of density overturns (Fig. 6.7). As the wave amplifies, the minimum Richardson number of the large-scale perturbation systematically decreases until the flow becomes locally susceptible to Kelvin–Helmholtz instabilities. The resulting intermittent density overturns in the regions of strong shear ($Ri < 1/4$) generate large Reynolds number convective turbulence, associated with large dissipation of heat

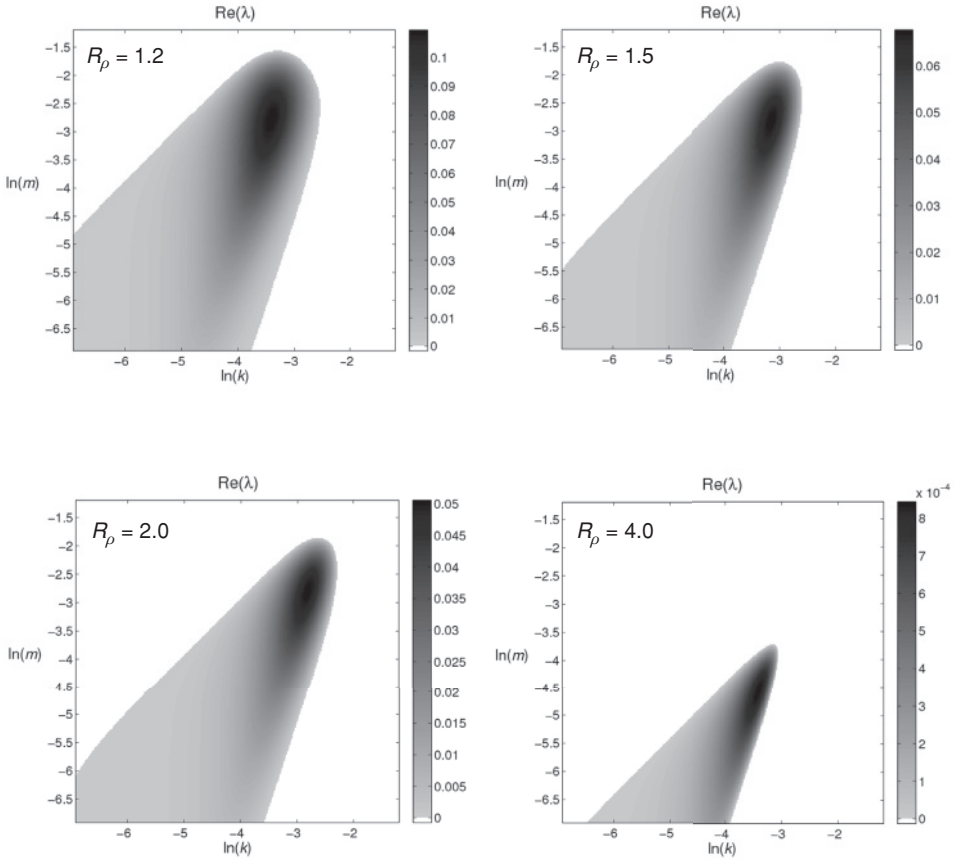

Figure 6.5 Growth rates (λ) of the collective instability waves as a function of the wavenumbers k and m for various values of the density ratio (R_ρ). Only the positive values of λ are shown. The unstable region shrinks when R_ρ is increased.

and momentum. While the connection between wave-induced overturns, turbulent patches and vertical mixing is well known (Gregg, 1987; Thorpe, 2005), such processes are usually discussed in the context of the mechanical generation of gravity waves by a combination of tidal forcing and topographic effects. The intriguing suggestion that some turbulent mixing events can be produced by the indirect action of double-diffusion (Stern *et al.*, 2001) warrants further analysis and quantification.

The nonlinear effects of collective instability have been examined more systematically by Stern and Simeonov (2002), who developed a fully nonlinear numerical parametric model of salt fingering. This model made no attempt to resolve individual salt fingers but represented their effects in terms of vertical fluxes (6.2). The parametric model was shown to be consistent with the DNS in the computationally accessible regimes. For more challenging large-scale configurations, beyond

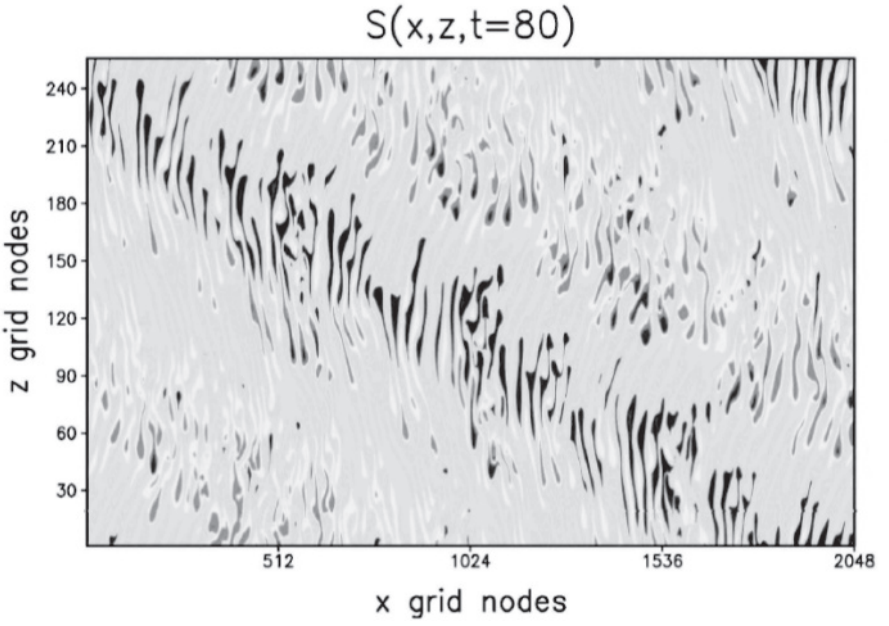

Figure 6.6 Two-dimensional direct numerical simulation showing salt fingers growing in the internal gravity wave. Presented is the departure of salinity from the uniform background gradient. Red color corresponds to high values and low values are shown in blue. From Stern *et al.* (2001). See color plates section.

the reach of DNS, the parametric model offered a unique opportunity to simulate numerically collective instability waves and the resulting overturns.

Numerical simulations in Stern and Simeonov (2002), both parametric and direct, confirmed the propensity of collective instability waves to overturn and generate localized patches of enhanced mixing. The intensity of these events was shown to be strongly dependent on the background density ratio. For large density ratios ($R_\rho > 2$), collective instability is relatively benign – it generates density overturns that are limited in size and magnitude and do not contribute significantly to the vertical transfer of properties. However, the situation changes dramatically for low density ratios ($R_\rho < 2$). In this case, the portion of the net heat flux transported by the collective instability waves is comparable to, or exceeds, the direct salt-finger flux. This result has potentially far-reaching implications for the analysis and interpretation of small-scale mixing in the ocean. So far, attempts to quantify the contribution of salt fingers to vertical mixing have been focused on the direct effects caused by the primary double-diffusive instabilities (e.g., St. Laurent and Schmitt, 1999). However, if collective instability waves are responsible for a significant fraction of net vertical transport, double-diffusive mixing would be effectively disguised as mechanically generated turbulence. To the best

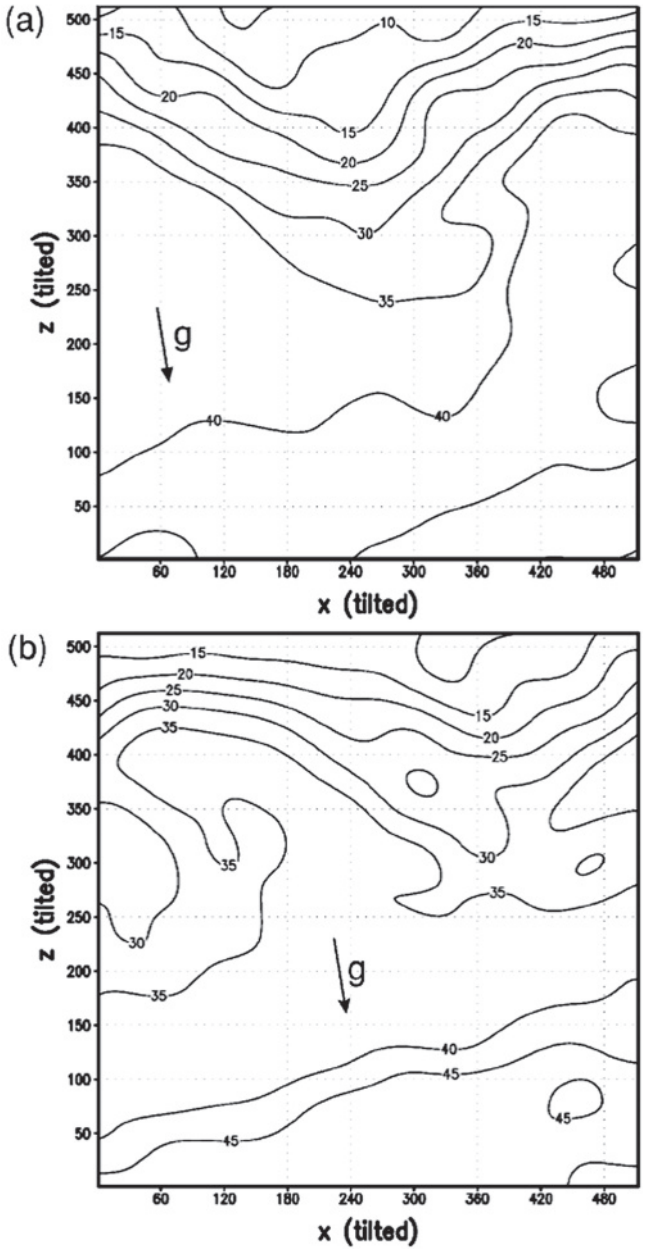

Figure 6.7 Total low-passed density distribution in the overturning collective instability wave. This direct numerical simulation was performed in the tilted coordinate system; the orientation of the gravity vector is indicated. The plots in (a) and (b) show the state shortly before and after the overturn, respectively. From Stern *et al.* (2001).

of our knowledge, this possibility has not yet been considered in the analysis of field data.

An interesting property of collective instability was identified by Radko and Stern (2011),[1] who suggested that their impact can be significantly enhanced by external large-scale shears, which are ubiquitous in the ocean. This somewhat counterintuitive conclusion was based on the stability analysis of a parallel sinusoidal shear flow in finger-favorable stratification. Salt fingers were introduced by parameterizing vertical fluxes (6.2), similar to the approach taken by Stern and Simeonov (2002). Linear stability analysis of this system revealed the existence of relatively large-scale instabilities driven by the interaction between the background shear and double-diffusion. These oscillatory thermohaline–shear modes can be interpreted as a form of the classical collective instability modes, modulated by the basic current. However, they appear to be much more effective in mixing, owing to their ability to interact with the background flow.

The importance of collective thermohaline–shear instabilities was confirmed by numerical three-dimensional simulations of the parametric model. Figure 6.8 presents the evolution of the temperature perturbation in an experiment initiated by dynamically stable shear with minimum Richardson number of $Ri = 0.5$. The background density ratio is $R_\rho = 2$, which is representative of the Atlantic thermocline. In dimensional units, the size of the computational domain in Figure 6.8 is $\sim 20\,\mathrm{m} \times 10\,\mathrm{m} \times 5\,\mathrm{m}$ and the duration is equivalent to a period of a few days. Calculations of this scale are currently beyond DNS capabilities and thus are only accessible by parameterized models. This experiment confirmed that the inclusion of double-diffusive fluxes immediately destabilizes the system. Consistent with linear inferences (Radko and Stern, 2011), the instability modes that appeared first (Fig. 6.8a) strongly varied in y and z but were almost uniform in the direction of the background current (x). This pattern changed dramatically in the later stages of the experiment; the development of significant along-current temperature variation is shown in Figure 6.8b. Note that the along-current variability at this stage is particularly strong at the locations of the largest background shear (bottom, center and top of each plot in Fig. 6.8).

The along-current perturbations in Figure 6.8b were interpreted as secondary Kelvin–Helmholtz instabilities induced by the thermohaline modes in the following manner. Growing collective instability modes introduced, upon reaching finite amplitude, significant spatial variation in the vertical density gradient. The reduction of density gradient in some regions, in turn, made the flow susceptible to local

[1] This was the final scientific contribution of Melvin Stern; the paper was completed after he passed away. Despite serious health problems, Melvin maintained keen interest in the dynamics of collective instabilities and was actively involved in this project until his last days.

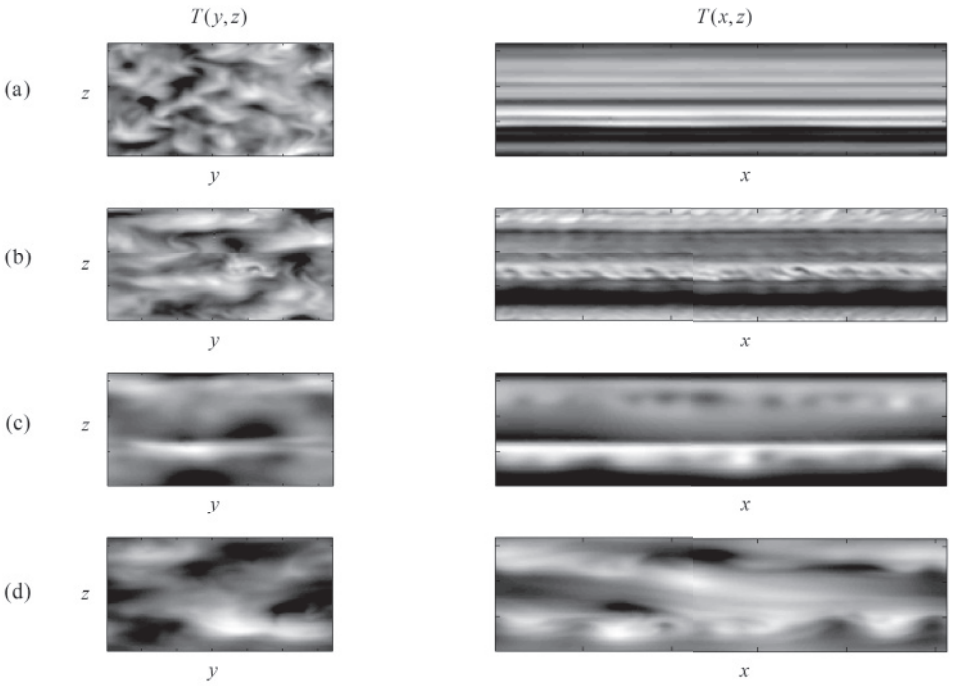

Figure 6.8 Numerical simulation of the subcritical ($Ri = 0.5$) double-diffusive shear flow. The (left) cross-current and (right) along-current vertical sections are shown at various times (increasing downward). Note rapid destabilization of the shear flow by double-diffusion. From Radko and Stern (2011).

Kelvin–Helmholtz instabilities, particularly in the zones of high background shear, resulting in intense convective mixing. However, the localization of secondary instabilities to the regions of strong shear was transient. The ensuing vertical mixing stabilized the high-shear zones and the along-current variability shifted to low-shear regions (Fig. 6.8c). In the final stage of the experiment (Fig. 6.8d) the temperature variance was distributed rather uniformly throughout the computational domain. Also apparent is the tendency for a systematic increase of typical spatial scales of the perturbation in time, associated with the sequential coalescence of relatively small eddies into larger and larger structures. Such mergers are common in turbulent stratified fluids (Balmforth *et al.*, 1998; Radko, 2007) particularly in the double-diffusive environment (Huppert, 1971; Radko, 2005; Simeonov and Stern, 2008). It should be emphasized that all the interesting turbulent dynamics illustrated in Figure 6.8 are ultimately driven by collective instabilities – in the absence of double-diffusion, the background flow would be stable.

In order to quantify the role of stable shear, the calculation in Figure 6.8 has been reproduced without the background current. The outcome was very different. The

removal of the background shear decreased the probability of density overturns by an order of magnitude and substantially reduced the average mixing rates. Thus, both background current and collective instabilities appear to be essential and mutually reinforcing in terms of transition to turbulence for dynamically stable configurations. Also revealing is the comparison of the $Ri = 0.5$ experiment in Figure 6.8 with its dynamically unstable counterpart ($Ri = 0.15$). The average heat flux by the resolved scales of motion (thus excluding the direct double-diffusive transport) in the experiment with $Ri = 0.5$ was comparable to but smaller, by a factor of three, than in the dynamically unstable ($Ri = 0.15$) calculation. This similarity suggests that, with respect to the generation of density overturns and consequent mixing, in the double-diffusive thermocline there is no dramatic difference between the low Ri and high Ri regimes. This proposition can help to rationalize some observations of turbulent mixing in the main thermocline, an environment generally characterized by relatively weak dynamically stable ($Ri > 1/4$) shears (e.g., Polzin, 1996).

In summary, collective instability provides an efficient mechanism for the generation and maintenance of an active wave environment and thus can indirectly influence vertical turbulent mixing. In addition to the spontaneous generation of internal waves from random perturbations, collective instability is likely to amplify a broad band of waves generated by other causes (e.g., topographic and tidal effects), thereby facilitating density overturns and transition to turbulence. The identification of such processes in nature is challenging and more work needs to be done to quantify the large-scale impact of collective instability. Another potentially critical mechanism for irreversible mixing in the ocean is related to the tendency of double-diffusion to drive quasi-lateral intrusions in the presence of horizontal temperature and salinity gradients. The dynamics of such interleaving motions are discussed next.